On Continuous-Set Model Predictive Control of Permanent Magnet Synchronous Machines

Issa Hammoud, *Student Member, IEEE*, Sebastian Hentzelt, Ke Xu, Thimo Oehlschlägel, Mohamed Abdelrahem, *Senior Member, IEEE*, Christoph Hackl, *Senior Member, IEEE*, and Ralph Kennel, *Senior Member, IEEE*

***Abstract*—This article presents a real-time realization of a continuous-control-set model predictive current controller for the two types of permanent magnet synchronous machines: 1) surface-mounted permanent magnet synchronous machine (SMPMSM) and 2) interior permanent magnet synchronous machine (IPMSM). The constrained optimization problem is solved online using a slack formulation of the primal-dual interior-point method. The proposed controller is tested on a 14.5 kW SMPMSM based on the linear time-invariant (LTI) model of the machine and on a 0.5 kW IPMSM. For the latter, we present in detail how the nonlinear first-principles modeling yields the fastest possible transient as well as an offset-free steady-state performance. The experimental results were obtained at sampling times typically used in the electrical drive applications (125 and 100 μs for the two machines, respectively).**

***Index Terms*—Continuous-control-set model predictive control (CCS-MPC), first-principles nonlinear modeling, interior-point (IP) based optimization, permanent magnet synchronous machines.**

I. Introduction

PERMANENT magnet synchronous motors (PMSMs) are broadly used in a wide range of industrial applications due to their advantageous characteristics, such as their compact design, high energy density and efficiency, reliability, and fast torque response [1]. High-performance current control is required for an optimal operation of PMSMs. Among others, model predictive control (MPC) has been extensively studied for this task [2]. MPC relies on a mathematical model that represents the dynamics of the plant under control in order to predict its response within a predefined prediction time horizon N. By minimizing a cost functional that describes the control objective, a parameterized control input sequence is to be found by solving an optimal control problem (OCP) subjected to an initial condition, corresponding system dynamics, and constraints of the system states and control inputs. The feedback is achieved in MPC by the receding horizon principle that at each sampling period, the prediction horizon is moved forward into the future by one step, while applying only the first control input from the obtained control sequence to the plant [3]. The general concept of discrete-time MPC is depicted in Fig. 1, where $\boldsymbol{U}$ is the sequence of control inputs, $\boldsymbol{Y}$ is the sequence of system outputs, and $\boldsymbol{Y}_{\text{ref}}$ is the sequence of reference outputs.

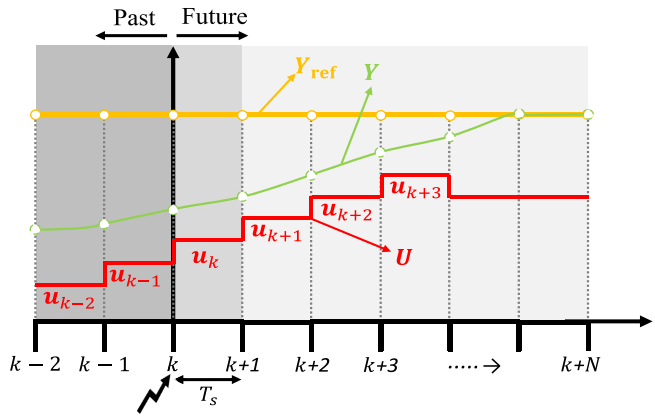

Fig. 1. General concept of discrete-time MPC with a prediction horizon length N.

Since the very early implementations of MPC schemes in the field of power electronics and electrical drives [4]–[6], the vast majority of publications have investigated the direct variant of MPC, which is finite-control-set model predictive control (FCS-MPC) [7]–[10]. In FCS-MPC, the OCP is solved by a combinatorial approach that evaluates the finite set of possible system transitions, governed by the finite set of output voltage vectors (VVs) of power converters.

Owing to the absence of a modulator, applying one VV at a complete sampling period as in the case with FCS-MPC results in relatively high ripples on the tracked states at typical

Manuscript received January 18, 2022; revised March 17, 2022; accepted March 24, 2022. Date of publication April 5, 2022; date of current version May 23, 2022. This work was supported by IAV GmbH, Gifhorn, Germany. Recommended for publication by Associate Editor J. Zhang. *(Corresponding author: Issa Hammoud.)*

Issa Hammoud is with the Institute for Electrical Drive Systems and Power Electronics, Technical University of Munich, 80333 Munich, Germany, and also with the Powertrain Mechatronics Control Engineering Excellence Cluster, IAV GmbH, 38518 Gifhorn, Germany (e-mail: issa.hammoud@tum.de).

Sebastian Hentzelt, Ke Xu, and Thimo Oehlschlägel are with the Powertrain Mechatronics Control Engineering Excellence Cluster, IAV GmbH, 38518 Gifhorn, Germany (e-mail: sebastian.hentzelt@iav.de; ke.xu@iav.de; thimo.oehlschlaegel@iav.de).

Mohamed Abdelrahem and Ralph Kennel are with the Institute for Electrical Drive Systems and Power Electronics, Technical University of Munich, 80333 Munich, Germany (e-mail: mohamed.abdelrahem@tum.de; ralph.kennel@tum.de).

Christoph Hackl is with the Laboratory for Mechatronic and Renewable Energy Systems, Munich University of Applied Sciences, 80335 Munich, Germany (e-mail: christoph.hackl@hm.edu).

Color versions of one or more figures in this article are available at https://doi.org/10.1109/TPEL.2022.3164968.

Digital Object Identifier 10.1109/TPEL.2022.3164968

sampling intervals, especially for low-inductance machines. To this end, FCS-MPC schemes need to operate at very high sampling frequencies in order to provide an acceptable steady-state performance. Experimental validation for the current control loop with FCS-MPC schemes for synchronous machines using field-programmable gate arrays (FPGAs) has recently been reported at 40 and 100 kHz in [11] and [12], respectively.

The other variant of MPC in power electronic applications is the indirect MPC. This variant is based on finding a continuous-time optimal VV either numerically by minimizing a cost functional in continuous-control-set model predictive control (CCS-MPC) or analytically by using a deadbeat function in deadbeat MPC. The continuous-time optimal VV is to be realized by using the adjacent VVs with corresponding timings via a modulation scheme. By doing this, the general advantages of MPC are kept, such as handling of constraints, incorporation of nonlinearities, fast dynamic response, and the use of multiobjective cost functions. This is achieved while obtaining a favorable steady-state performance, albeit at the expense of having more switching efforts due to the use of a modulator. The key performance differences between direct and indirect MPC are as follows:

1) When sampled at the same frequency, CCS-MPC yields significantly less current ripples than FCS-MPC [13].
2) In transients, despite that indirect MPC methods can reach the new reference state at the end of only one sampling step, FCS-MPC when sampled at significantly higher frequencies can provide faster dynamic response.[1,2]

To clarify these differences, a simulative study is carried out for the current control of an interior permanent magnet synchronous machine (IPMSM), where a conventional FCS-MPC controller with a sampling frequency $f_{\text{sa}} = 100$ kHz with no penalty on the switching effort in the cost function and a CCS-MPC controller with a sampling frequency $f_{\text{sa}} = 10$ kHz are compared. The results are depicted in Fig. 2(a) for FCS-MPC, in Fig. 2(b) for CCS-MPC with a current measurement at each switching state transition within the sampling period [eight sampling points at each sampling period T_s for the used symmetrical space vector modulation (SVM)], and in Fig. 2(c) for CCS-MPC with only one current measurement at the middle of each sampling period. On the one hand, it can be observed that FCS-MPC has significantly higher ripples, albeit that it was sampled at a ten times higher sampling. On the other hand, even though CCS-MPC has reached the new reference current amplitude in only one sampling interval of $T_s = 100\ \mu$s, FCS-MPC has reached it in only 40 μs, despite in four sampling periods.

Methods to combine these two contradictory objectives in electrical drive systems of having the fastest possible dynamics with respect to the physical limit of the plant and an optimal steady-state performance in terms of minimal ripples and total harmonic distortion (THD) content were proposed in the literature. Proposals along these lines include model predictive pulse pattern control (MP^{3}C) [10], [14], which adopts MPC to obtain a deadbeat-like fast transient performance with optimal precomputed pulse patterns in steady-state operation [15]. Another proposal in the same direction is the variable-switching-point model predictive control (VSP-MPC) [16]–[18], in which the optimal VV is not being applied at equidistant intervals

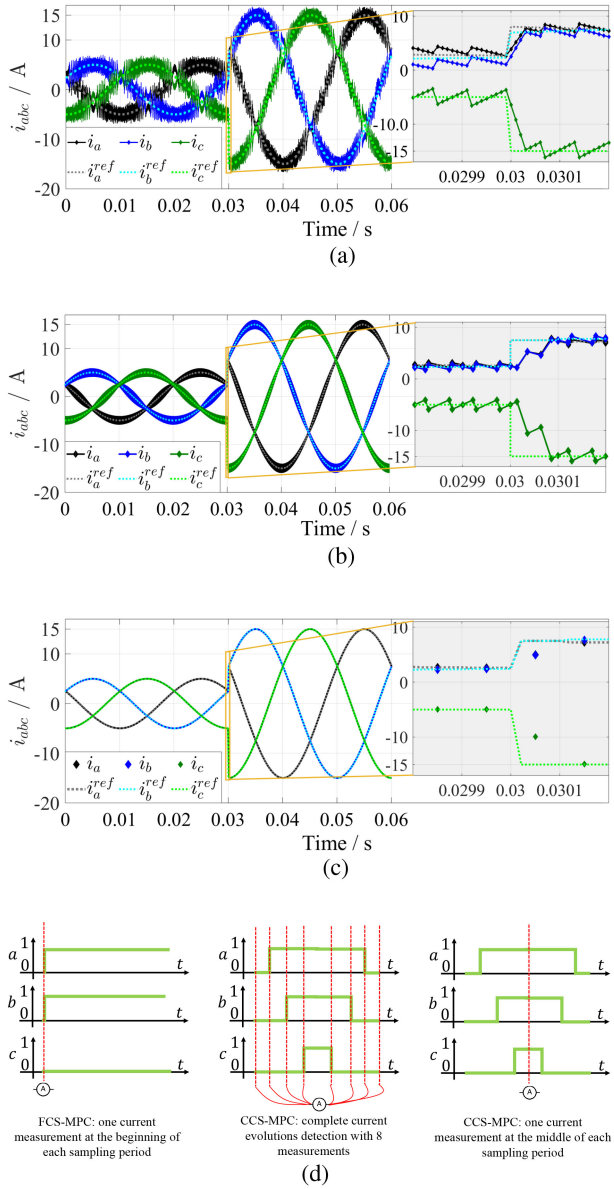

Fig. 2. Example to illustrate the conceptual difference in transients and steady-state ripple between FCS-MPC and CCS-MPC applied for the current control of a synchronous machine. (a) FCS-MPC with $f_{\text{sa}} = 100$ kHz, and the current is measured once at the beginning of each sampling interval. (b) CCS-MPC with $f_{\text{sa}} = 10$ kHz, and the current is measured eight times at each transition within a PWM cycle within each sampling period. (c) CCS-MPC with $f_{\text{sa}} = 10$ kHz, and the current is measured only once at the middle of each sampling period. (d) Sketch to illustrate where the current is being measured within the sampling period and the symmetrical SVM.

[1]The nature of solving the FCS-MPC problem by enumeration approaches makes it possible to benefit from parallel computations by using FPGAs and, hence, achieve extremely fast sampling times in contrary to CCS-MPC.

[2]For a comprehensive understanding of this fact, the resolution of current measurements needs to be high enough to detect the complete state's evolution within one sampling period corresponding to each switching transition. This can be easily done in simulation as presented in Fig. 2(b); however, in practice, the current is mostly measured only once at the middle of the sampling period, which is applied in the experimental part throughout this article.

as with the conventional FCS-MPC, but at a variable switching point in time, which consequently reduce the steady-state ripples while keeping the fast dynamic performance that characterizes direct control methods. However, the offline optimization leads to losing the sense of accountability for unseen disturbances/faults/model mismatches in MP^{3}C, and applying only one VV at each sampling period leads to nonminimal ripples and THD in the steady-state in VSP-MPC. In [19], a recent and comprehensive review of the different MPC methods in electrical drive applications was presented.

To this end, CCS-MPC is attractive as long as a mathematical model that represents the nonlinear drive system behavior in the whole operating range is available [20], and an efficient numerical solver is able to iteratively evaluate the model online in the submillisecond sampling time range.

Solving the underlying OCP with CCS-MPC in real time in the submillisecond range is challenging. This has limited the number of real-time implementations of CCS-MPC schemes in the literature. A nonlinear MPC scheme was presented based on the Lagrangian method in combination with a real-time gradient method using the framework *grampc* with a sampling time of 500 μs for IPMSMs in [21] and for induction machines in [22]. In [23] and [24], an active-set solver for the quadratic programming problem considering input and state constraints of an isotropic synchronous motor with a sampling time of 300 μs was proposed, however, assuming a linear time-invariant (LTI) model. In [25], a nonlinear MPC scheme using the framework *acado* was presented for synchronous reluctance machines with a sampling time of 250 μs. The proposed CCS-MPC scheme in this article is implemented experimentally with the sampling times of 125 and 100 μs for a surface-mounted permanent magnet synchronous machine (SMPMSM) and an IPMSM, respectively. The contributions of this article are as follows:

1) A thorough nonlinear modeling of the PMSM drive system is presented, which is essential for the optimal performance of model-based control, in contrary to the mostly used simple LTI models. This includes the PMSM model parameter identification, the inverter nonlinearity and the inevitable angle delay compensation (ADC), and the measurement synchronization. Moreover, a compact literature survey about integral action approaches with MPC in electrical machine control is included.
2) An efficient numerical solver based on a slack formulation of the primal-dual interior-point (IP) method to solve the underlying constrained OCP of the CCS-MPC for PMSMs is proposed.
3) Experimental results on an IPMSM and an SMPMSM prove the validity and effectiveness of the proposed modeling procedure and control scheme.

II. Mathematical Modeling

In this section, the generic model of the two-level voltage-source inverter (VSI) is presented, and its voltage drop is analyzed and compensated. Furthermore, the generic model of PMSMs is introduced in the rotating dq reference frame [26], and the state-of-the-art procedure to identify the model parameters is presented.

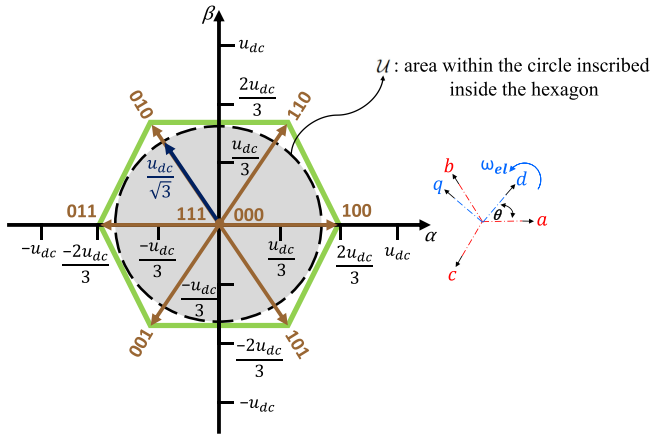

Fig. 3. Output VVs of a two-level VSI in the stationary $\alpha - \beta$ plane.

A. Two-Level Inverter

Direct-to-alternating power converters have a finite set of output VVs. Thus, the control input vector

$$\boldsymbol{u}_k \in \{\boldsymbol{u}_1, \ldots, \boldsymbol{u}_m\} \tag{1}$$

where m is the number of output VVs of the power converter under consideration, and $m = 8$ for the two-level VSI. The ac-side voltage of the inverter $\boldsymbol{u}^f_{abc}$ is determined with respect to the dc-link voltage u_{dc} based on the switching states vector $\boldsymbol{s}_{abc} = (s_a, s_b, s_c)^\top$, where $s_p \in \{0, 1\}$ for $p \in \{a, b, c\}$ [27]. The finite output VVs of a two-level VSI are depicted in Fig. 3. In practice, the semiconducting switches that form the power modules of the inverter are exposed to a nonideal and nonlinear switching behavior. Therefore, a deviation between the commanded and measured VVs exists. To illustrate this effect, the shaft of the IPMSM was locked, and commanded reference VVs that cover the whole $\alpha - \beta$ plane have been applied. The motor stator resistance is measured to be 38.5 mΩ and is assumed to be constant. The measured currents are shown in black in Fig. 4(a), where the commanded reference currents, which are computed from the commanded VVs and the known resistance, are shown in green. A clear mismatch can be observed in Fig. 4(a). The state-of-the-art method to compensate for this effect is to obtain a phase-voltage compensation curve as a function of the phase current and to use it as a lookup table (LUT) feedforward compensation in the model-based control. To do so, one phase voltage is kept at 0 V, the second phase voltage gets ascending reference voltages, while the third phase gets descending references. The real obtained voltage at each reference is then computed from the three-phase measured currents and the known stator resistance. This test is repeated with the other two possible phase combinations. The obtained missing phase-voltage compensation curves are shown in Fig. 4(b). In Fig. 4(c), the results after the compensation are shown in a grid of 928 VVs that covers the whole $\alpha - \beta$ plane.

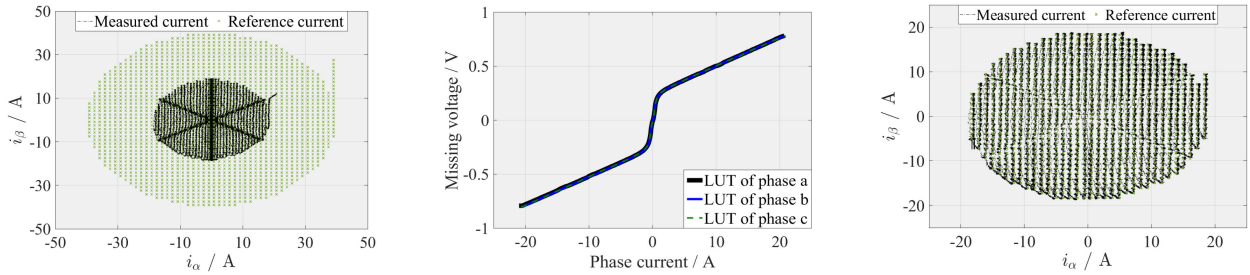

Fig. 4. Braked-motor test to illustrate the effect of the voltage drop in a two-level VSI. (a) Reference and measured current vectors—inverter voltage drop effect. (b) VSI missing voltage as a function of the phase current in the *abc* frame. (c) Reference and measured current vectors—with the compensation.

B. Permanent Magnet Synchronous Machine

The mathematical model of a three-phase PMSM in the rotating dq reference frame is expressed as [28]

$$u_d = R_s i_d + \frac{d}{dt}\psi_d^{(i_d,i_q)} - \omega_{\text{el}}\psi_q^{(i_d,i_q)} \tag{2a}$$

$$u_q = R_s i_q + \frac{d}{dt}\psi_q^{(i_d,i_q)} + \omega_{\text{el}}\psi_d^{(i_d,i_q)} \tag{2b}$$

where

$$\psi_d^{(i_d,i_q)} = \psi_p^{(i_q)} + L_d^{(i_d,i_q)} i_d \tag{3a}$$

$$\psi_q^{(i_d,i_q)} = L_q^{(i_d,i_q)} i_q \tag{3b}$$

$$\frac{d}{dt}\psi_d = \frac{d}{dt}\psi_p + L_{dd}^{(i_d,i_q)}\frac{di_d}{dt} + L_{dq}^{(i_d,i_q)}\frac{di_q}{dt} \tag{3c}$$

$$\frac{d}{dt}\psi_q = L_{qq}^{(i_d,i_q)}\frac{di_q}{dt} + L_{qd}^{(i_d,i_q)}\frac{di_d}{dt} \tag{3d}$$

and $\psi_p^{(i_q)}$ equals $\psi_d^{(i_d=0,i_q)}$. The absolute and differential inductances are current dependent. The absolute inductances are defined as

$$L_d^{(i_d,i_q)} = \frac{\psi_d^{(i_d,i_q)} - \psi_p^{(i_q)}}{i_d} \tag{4a}$$

$$L_q^{(i_d,i_q)} = \frac{\psi_q^{(i_d,i_q)}}{i_q} \tag{4b}$$

where the differential inductances are defined as the partial derivatives of the fluxes along the currents

$$L_{dd}^{(i_d,i_q)} = \frac{\partial\psi_d}{\partial i_d} \quad \text{(5a)} \qquad L_{dq}^{(i_d,i_q)} = \frac{\partial\psi_d}{\partial i_q} \quad \text{(5b)}$$

$$L_{qd}^{(i_d,i_q)} = \frac{\partial\psi_q}{\partial i_d} \quad \text{(5c)} \qquad L_{qq}^{(i_d,i_q)} = \frac{\partial\psi_q}{\partial i_q}. \quad \text{(5d)}$$

To this end, substituting (3) into (2) yields the nonlinear model of PMSMs. However, to facilitate the numerical optimization in real-time in the available submillisecond sampling time range, the following assumptions can be realistically made:

1) The time derivative of the permanent magnet flux linkage $\frac{d}{dt}\psi_p$ is set to be zero [28].
2) The cross-saturation is to be neglected. Hence, the mutual differential inductances L_{dq} and L_{qd} tend to zero [29]. This has a minor effect in prediction as their values are typically one order of magnitude less than self-differential inductances L_{dd} and L_{qq} [30].
3) The self differential inductances L_{dd} and L_{qq} are highly correlated with the absolute inductances L_d and L_q [28]. Slight differences occur only at high motor speeds. Thus, it is assumed that $L_{dd} \approx L_d$ and $L_{qq} \approx L_q$ [21].

With these three simplifications, the nonlinear dynamic model of PMSMs is expressed as

$$u_d = R_s i_d + L_d\frac{di_d}{dt} - \omega_{\text{el}} L_q i_q \tag{6a}$$

$$u_q = R_s i_q + L_q\frac{di_q}{dt} + \omega_{\text{el}} L_d i_d + \omega_{\text{el}}\psi_p \tag{6b}$$

where u_d and u_q are the stator voltages (in volts), i_d and i_q are the stator currents (in amperes), L_d and L_q are the current-dependent inductances (in henries) (for SMPMSM $L_d = L_q$, where for IPMSM $L_d \neq L_q$ [27]), R_s is the stator resistance (in ohms), ψ_p is the permanent magnet flux linkage (in weber) and is a function of i_q, and ω_{el} is the electrical angular speed (in rad $\cdot$ s^{-1}), $\omega_{\text{el}} = n_p\omega_{\text{me}}$, where n_p is the number of pole pairs, and ω_{me} is the mechanical rotor speed (in rad $\cdot$ s^{-1}).

For the MPC controller design, the system dynamics (6) are discretized using the explicit Euler discretization method with a sampling time T_s. The discrete time-variant model is expressed in the state-space representation such as

$$\boldsymbol{x}_{k+1} = \boldsymbol{A}_k\boldsymbol{x}_k + \boldsymbol{B}_k\boldsymbol{u}_k + \boldsymbol{g}_k, \boldsymbol{x}_0 = \tilde{\boldsymbol{x}}_0 \tag{7a}$$

$$\boldsymbol{y}_k = \boldsymbol{C}\boldsymbol{x}_k \tag{7b}$$

where k represents the discrete time index; $\tilde{\boldsymbol{x}}_0$ is the measurement at the beginning of the prediction interval; $\boldsymbol{x} \in \mathbb{R}^{N_x}$, $\boldsymbol{u} \in \mathbb{R}^{N_u}$, and $\boldsymbol{y} \in \mathbb{R}^{N_y}$ are the state, input, and output vectors with N_x, N_u, and N_y as the number of states, inputs, and outputs, respectively; $\boldsymbol{A}_k$ and $\boldsymbol{B}_k$ are the time-variant system matrices;

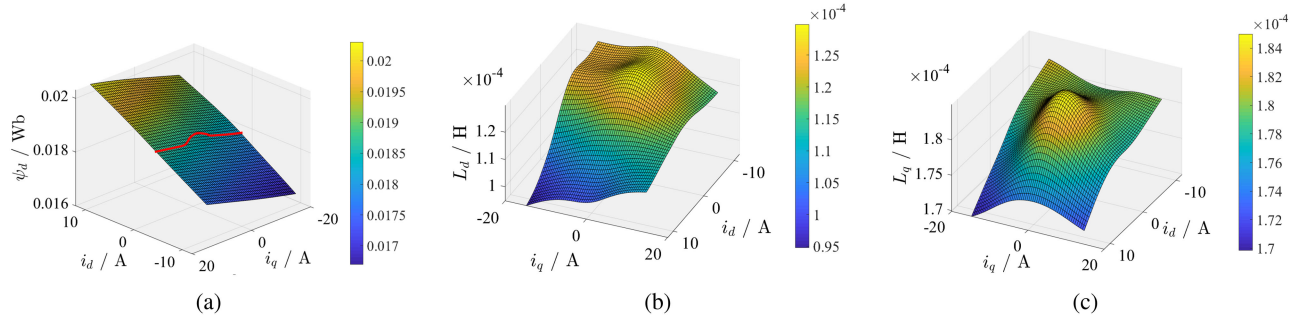

Fig. 5. Obtained parameters maps. (a) $\psi_p = \psi_d^{(i_d=0,i_q)}$ (in red). (b) d-axis inductance. (c) q-axis inductance.

and $\boldsymbol{C}$ is the output matrix, and defined as[3]

$$\boldsymbol{A}_k = \begin{bmatrix} 1 - \frac{T_s R_s}{L_{d,k}} & \frac{L_{q,k}}{L_{d,k}} T_s \omega_{el,k} \\ -\frac{L_{d,k}}{L_{q,k}} T_s \omega_{el,k} & 1 - \frac{T_s R_s}{L_{q,k}} \end{bmatrix}, \boldsymbol{x}_k = \begin{pmatrix} i_{d,k} \\ i_{q,k} \end{pmatrix}$$

$$\boldsymbol{B}_k = \begin{bmatrix} \frac{T_s}{L_{d,k}} & 0 \\ 0 & \frac{T_s}{L_{q,k}} \end{bmatrix}, \boldsymbol{u}_k = \begin{pmatrix} u_{d,k} \\ u_{q,k} \end{pmatrix}, \boldsymbol{g}_k = \begin{pmatrix} 0 \\ -\frac{T_s \omega_{el,k} \psi_{p,k}}{L_{q,k}} \end{pmatrix}$$

$$\boldsymbol{C} = \begin{bmatrix} 1 & 0 \\ 0 & 1 \end{bmatrix}, \boldsymbol{y}_k = \begin{pmatrix} i_{d,k} \\ i_{q,k} \end{pmatrix}. \tag{8}$$

The standard procedure to identify the current-dependent parameters (L_d, L_q, ψ_p) in model (8) is to control the motor shaft speed via a load motor and to inject reference steady-state currents in the complete $i_d - i_q$ plane with an appropriate grid resolution. The stator resistance is to be measured, and then, the fluxes can be computed at each steady-state point as

$$\psi_d = \frac{u_q - R_s i_q}{\omega_{\text{el}}} \tag{9a}$$

$$\psi_q = -\frac{u_d - R_s i_d}{\omega_{\text{el}}}. \tag{9b}$$

Then, the absolute inductances can be calculated as in (4). For the IPMSM used in the experimental validation in this article, the parameters are identified using the aforementioned procedure at $\omega_{\text{me}} = 500$ r/min with a grid resolution of 0.5 A. The obtained parameters maps are smoothed with the spline interpolation method [32] and are depicted in Fig. 5.

C. Measurement Synchronization

The current is being measured at the middle of each sampling period T_s, while the voltage is being applied at the end of one sampling period/beginning of the upcoming one. This misalignment between the time instant when the computed voltage is applied and the current is measured must be compensated for in prediction for control as well as in parameter estimation and model identification [33]. For prediction in control, once a prediction model is available, this comes in the form of initial condition correction for the system states. This is done by predicting the values of the states half a cycle ahead, i.e.,

$$\boldsymbol{x}_k = \tilde{\boldsymbol{x}}_k + \frac{T_s}{2} \boldsymbol{f} \tag{10}$$

with the system dynamics vector $\boldsymbol{f}$ defined as

$$\begin{pmatrix} f_d \\ f_q \end{pmatrix} = \frac{d\boldsymbol{x}}{dt} = \begin{pmatrix} \frac{-R_s i_d}{L_d} + \frac{L_q \omega_{\text{el}} i_q}{L_d} + \frac{u_d}{L_d} \\ \frac{-R_s i_q}{L_q} - \frac{L_d \omega_{\text{el}} i_d}{L_q} + \frac{u_q}{L_q} - \frac{\omega_{\text{el}} \psi_p}{L_q} \end{pmatrix}. \tag{11}$$

By this, the effect of applying $\boldsymbol{u}_{k-1}$ for the upcoming half sampling period since the current was measured is compensated for. This is illustrated in Fig. 6. This is the measurement synchronization used in this article.

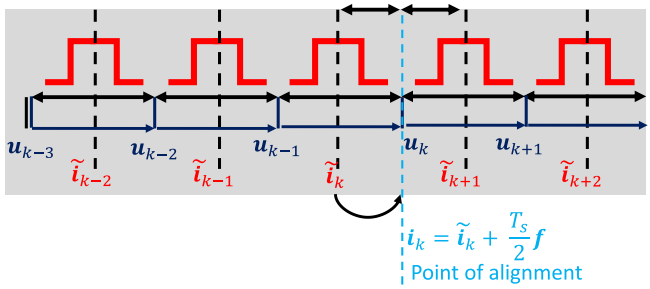

Fig. 6. Aligning the current measurement with the computed voltage by predicting its value half a cycle ahead and using the predicted value as an initial state in the MPC scheme.

D. Angle Delay Compensation

Owing to the needed signal processing time for the digital implementation of control schemes, an inevitable time delay occurs and causes an undesirable voltage mismatch [34]. In the dq frame, this comes in a form of rotating speed-dependent error VV. This effect can be observed by injecting a zero current in the d and q axes, and increasing the motor speed via the load machine while observing the needed stator voltage to maintain the zero current. When no ADC is considered, a deviation between the regulator voltages and their references occurs. The reference voltages to inject zero current can be computed directly by setting the currents and their derivatives to zero in (6), resulting in

$$u_d^{\text{ref}} = 0 \tag{12a}$$

$$u_q^{\text{ref}} = \omega_{\text{el}} \psi_p. \tag{12b}$$

[3]In FCS-MPC, in order to allow the direct penalization of the average switching frequency, the state prediction equation is typically expressed as $\boldsymbol{x}_{k+1} = \boldsymbol{A}_k \boldsymbol{x}_k + \boldsymbol{B}_k \boldsymbol{P}_k \boldsymbol{u}_k + \boldsymbol{g}_k$, with $\boldsymbol{P}$ and $\boldsymbol{u}_k$ being defined as in [31], and all other vectors and matrices being consistent with (8).

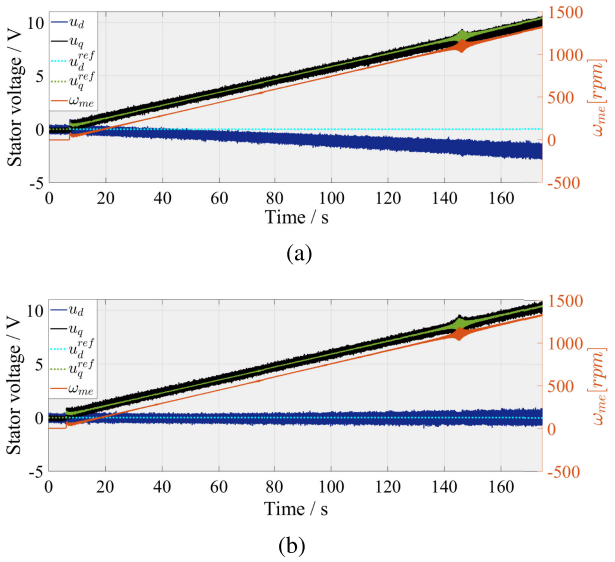

Fig. 7. Injecting zero current with increasing the shaft speed via the load machine. Stator voltages and their references and the measured speed (a) without ADC and (b) with ADC.

This affects the d-axis more significantly, as can be seen in Fig. 7(a). The state-of-the-art method to compensate for this delay is to add a speed-dependent angle compensation term of $1.5T_s\omega_{\text{el}}$ when converting the optimal VV from the controller to the inverter duty cycles. This compensation method is referred to as phase advancing compensation [34]. The test is repeated with this compensation, and the computed voltages are aligned with their references, as shown in Fig. 7(b).

E. Integral Action

Whether a simple LTI or a more complex nonlinear model of the drive system is incorporated within the model-based control design, modeling errors do exist. Hence, an integral action functionality is always needed. To enhance the robustness of MPC schemes against modeling mismatches, several approaches were proposed in the literature:

1) *discrete-time integrator* that is computed from a feedback loop with the measured outputs and their setpoints and is used as an additive control input added to the MPC control input [35], [36];
2) $\delta\boldsymbol{u}$ *formulation* of the OCP or the use of incremental state-space models with inductance observers [36]–[38];
3) *state-space model augmentation* with a disturbance or integral state $\boldsymbol{d}$. The model augmentation can be in the form of discrete-time integrators [39] or the most common choice of a fictitious integrating disturbance model [40]–[43]. This method was implemented with FCS-MPC in [44] and [45], with a constrained CCS-MPC in [25], and with an unconstrained CCS-MPC in [46]. A recent review of disturbance observers for MPC in electrical drives applications is made in [47];
4) *persistence step disturbance compensation* deals with incorrect steady-state gains yielded from the difference between the real model and the one used in the MPC formulation. This discrepancy is subtracted from the reference trajectory, and this yields an offset-free performance for asymptotically stable systems [48]. This approach was applied with a CCS-MPC controller in [24].
5) *online parameter estimation* of the fixed-structure model used in the controller online. For this purpose, different estimation techniques were proposed, such as recursive least squares, extended and unscented Kalman filters, and moving horizon estimators, to mention a few. A detailed overview of these parameter estimation approaches for PMSMs can be found in [49]–[51] and the references therein.

To this end, the aforementioned methods are extensively investigated in the literature to be combined with model-based controllers for electrical drives while using simple LTI models and choosing to abandon the inclusion of easy-to-include knowledge about the hardware (i.e., ADC, inverter nonlinearity compensation, and measurement synchronization). Despite the simplicity of this choice, and that it can assure an offset-free performance in the steady state, neglecting the possible inclusion of the nonlinear model yields a poor or at least suboptimal dynamic performance and higher ripples on the tracked states. This article is meant to motivate the use of nonlinear models and the known knowledge about the drive systems within model-based controllers. By doing so, it is shown in the experimental results section that the fastest possible transient performance with respect to the available control inputs and sampling frequency can be achieved in PMSM drive systems. The proposed nonlinear model-based CCS-MPC scheme is real-time implementable within the 100 μs sampling time typically available in such an application.

III. Continuous-Control-Set Model Predictive Control

The real-time implementation of the CCS-MPC controller relies on two main pillars: a proper mathematical model that represents the system dynamics, and an efficient numerical solver. In the previous section, we showed the procedure of obtaining such a model based on physical first-principle laws. A recent promising alternative is to obtain data-driven models purely from measurements using artificial intelligence methods [20], [33]. In this section, an efficient numerical solver is proposed to solve the underlying optimization problem in real-time, thereby addressing a major reason of the considerable less attention in the community toward the CCS-MPC variant of MPC in power electronic applications over FCS-MPC.

A. Problem Formulation

The standard control objectives for the current control task of PMSMs are to penalize the deviation of the stator currents from their references and the rate of change of the control inputs. These objectives are formulated in the standard cost function,

such as

$$J(\boldsymbol{u}) = \frac{1}{2}\sum_{i=0}^{N-1}(\boldsymbol{y}_{k+1+i} - \boldsymbol{r}_{k+1+i})^\top \boldsymbol{Q}(\boldsymbol{y}_{k+1+i} - \boldsymbol{r}_{k+1+i}) + \Delta\boldsymbol{u}_{k+i}^\top \boldsymbol{R}\Delta\boldsymbol{u}_{k+i} \tag{13}$$

with $\boldsymbol{Q} = \boldsymbol{Q}^\top \succeq 0$ and $\boldsymbol{R} = \boldsymbol{R}^\top \succ 0$ being the weighting matrices to weight the different control objectives accordingly with the appropriate dimensions. The vector $\boldsymbol{r}_{k+1+i}$ is the reference vector of the system outputs, $\Delta\boldsymbol{u}_{k+i} = (\boldsymbol{u}_{k+i} - \boldsymbol{u}_{k+i-1})^\top$ is the vector of the control input increments, and N represents the length of the prediction horizon.

The hexagonal voltage constraints formed by the discrete VVs of the inverter in the $\alpha - \beta$ and $d - q$ reference frames can be approximated by the inner circle inscribed within the hexagon in indirect control, as depicted in Fig. 3, such that at any discrete time instant, the following holds:

$$\sqrt{u_{d,k}^2 + u_{q,k}^2} \leq \frac{u_{\mathrm{dc}}}{\sqrt{3}}. \tag{14}$$

To prevent overheating, and for an optimal operation of the drive components (the battery, the inverter, and the motor itself), current constraints are imposed as

$$\sqrt{i_{d,k}^2 + i_{q,k}^2} \leq I_{\max}. \tag{15}$$

To this end, the OCP is stated as

$$\min_{\boldsymbol{u}} \quad J(\boldsymbol{u}) \tag{16a}$$

$$\text{s.t.} \quad (7a), (7b), (14), (15). \tag{16b}$$

B. IP Solver

In this section, the numerical solver used to simplify and find an approximate solution of the stated optimization problem in (16) in real time is presented. The solver is based on a slack formulation of the primal-dual IP method [52]. For the sake of generality, the dimensions of the zero and identity matrices ($\boldsymbol{O}$ and $\boldsymbol{I}$, respectively) are explicitly defined. The barrier parameter τ is fixed as in [53], and the maximum allowed number of iterations of the solver as well as the maximum possible line-search evaluations are limited. These settings yielded the expected performance in a real-time-capable manner within the available sampling time. At the beginning of each sampling period, the solver starts with an initial guess of $\boldsymbol{\xi}_k$ as the decision variables vector. After that, the Karush–Kuhn–Tucker (KKT) system of equations is built iteratively with the actual values of $\boldsymbol{\xi}_k$, $\boldsymbol{\mu}_k$, $\boldsymbol{\lambda}_k$, and $\boldsymbol{s}_k$, as a primal variable vector, dual variable vectors, and a slack variable vector, respectively. After solving the KKT system, a Newton direction is decided and a line search is to be performed in order to assure progress in each iteration. The variable α is scaled down iteratively within the line-search loop until the inequality constraint elements of the dual variable or the slack variables are positive. Once α is determined, a Newton step is taken, and the updated decision variable vector is computed. The algorithm is presented in Algorithm 1. The variables n_ξ, n_i, and n_e represent the number of decision variables, inequality constraints, and equality constraints, respectively. The Lagrangian is denoted as $\mathcal{L}$ and is defined as

$$\mathcal{L} = J(\boldsymbol{\xi}) + \boldsymbol{\lambda}^\top g(\boldsymbol{\xi}) + \boldsymbol{\mu}^\top h(\boldsymbol{\xi}) \tag{17}$$

where its Hessian is denoted with $\boldsymbol{H}$. The $.*$ operation is used to denote elementwise multiplication. A further speedup of the algorithm can be made by solving the KKT system more efficiently based on the result from [54]. A schematic diagram of the CCS-MPC scheme is shown in Fig. 8.

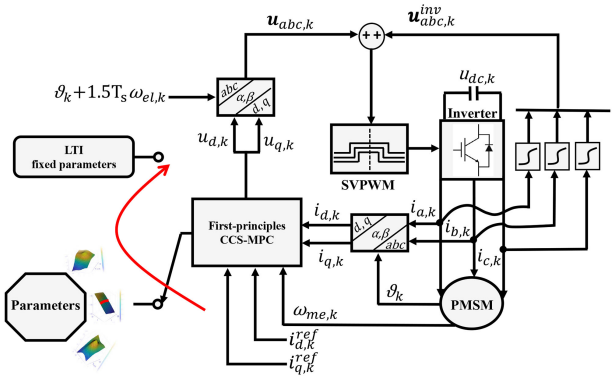

Fig. 8. Proposed CCS-MPC scheme.

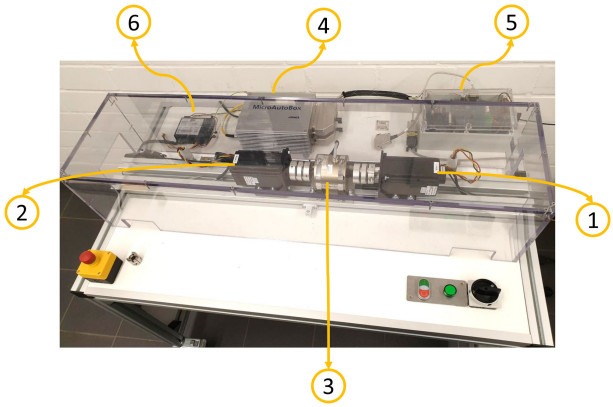

Fig. 9. IPMSM test bench: 1) main motor (IPMSM); 2) load motor (IPMSM); 3) torque sensor; 4) dSPACE Microautobox II; 5) two-level VSI from Texas Instruments and current and dc-link voltage sensors and measurements board; and 6) Ottbox commercial speed regulator for the load motor.

IV. Experimental Results

In this section, an experimental implementation of the CCS-MPC scheme for the current control task of PMSMs based on the proposed numerical solver is presented. First, it is tested based on the detailed nonlinear model obtained in Section II on a 500 W IPMSM. Second, an experimental validation on a 14.5 kW SMPMSM with a simple LTI model is presented.

A. Nonlinear CCS-MPC for an IPMSM

The test bench is depicted in Fig. 9. It consists of two IPMSMs coupled via a torque sensor. The load machine is speed-regulated and is driven by a commercial Ottbox controller. The main motor is current-regulated, and is fed by a two-level VSI from Texas

Algorithm 1: Primal-Dual Interior-Point solver.

Input: $\boldsymbol{\xi}_k$

Initialize τ, $\boldsymbol{\mu}_k = \boldsymbol{I}(n_i, 1)$, $\boldsymbol{s}_k = \boldsymbol{I}(n_i, 1)$, $\boldsymbol{\lambda}_k = \boldsymbol{I}(n_e, 1)$

for $i = 1$ *to* $MaxIter$ **do**

> Evaluate $\boldsymbol{H}$, $\boldsymbol{g}$, $\boldsymbol{h}$, $\nabla\boldsymbol{g}$, $\nabla\boldsymbol{h}$, $\nabla\boldsymbol{J}$, and $\boldsymbol{r}_T$

> Build the KKT system of equations

$$\begin{bmatrix} \boldsymbol{H}(\boldsymbol{\xi}_k, \boldsymbol{\mu}_k, \boldsymbol{\lambda}_k) & \nabla\boldsymbol{g}(\boldsymbol{\xi}_k) & \nabla\boldsymbol{h}(\boldsymbol{\xi}_k) & \boldsymbol{O}(n_\xi, n_i) \\ \nabla\boldsymbol{g}(\boldsymbol{\xi}_k)^\top & \boldsymbol{O}(n_e, n_e) & \boldsymbol{O}(n_e, n_i) & \boldsymbol{O}(n_e, n_i) \\ \nabla\boldsymbol{h}(\boldsymbol{\xi}_k)^\top & \boldsymbol{O}(n_i, n_e) & \boldsymbol{O}(n_i, n_i) & \boldsymbol{I}(n_i, n_i) \\ \boldsymbol{O}(n_i, n_\xi) & \boldsymbol{O}(n_i, n_e) & diag(\boldsymbol{s}) & diag(\boldsymbol{\mu}) \end{bmatrix} \begin{bmatrix} \Delta\boldsymbol{\xi} \\ \Delta\boldsymbol{\lambda} \\ \Delta\boldsymbol{\mu} \\ \Delta\boldsymbol{s} \end{bmatrix} = -\boldsymbol{r}_T \text{ ,with}$$

$$\boldsymbol{r}_T = \begin{bmatrix} \nabla\boldsymbol{J}(\boldsymbol{\xi}_k) + \nabla\boldsymbol{g}(\boldsymbol{\xi}_k)\boldsymbol{\lambda}_k + \nabla\boldsymbol{h}(\boldsymbol{\xi}_k)\boldsymbol{\mu}_k \\ \boldsymbol{g}(\boldsymbol{\xi}_k) \\ \boldsymbol{h}(\boldsymbol{\xi}_k) + \boldsymbol{s}_k \\ \boldsymbol{v}_k . * \boldsymbol{s}_k - \tau \end{bmatrix}$$

> Solve the KKT system of equations, and obtain a Newton direction $\begin{bmatrix} \Delta\boldsymbol{\xi} & \Delta\boldsymbol{\lambda} & \Delta\boldsymbol{\mu} & \Delta\boldsymbol{s} \end{bmatrix}^\top$.

> Compute the scaling factor $\alpha \in]0, 1]$ by line search.

> Initialize $\alpha = 1$, and it's reduction scaler $0 < k_{ls} < 1$

for $j = 1$ *to* $MaxIterLineSearch$ **do**

> Compute an iterative step:

$$\boldsymbol{\mu}_t = \boldsymbol{\mu}_k + \alpha\Delta\boldsymbol{\mu},$$
$$\boldsymbol{s}_t = \boldsymbol{s}_k + \alpha\Delta\boldsymbol{s};$$

Check **if** $\boldsymbol{\mu}_t > 0$ *and* $\boldsymbol{s}_t > 0$ **then**

break; (fix α)

end

> Decrease α:

$$\alpha = \alpha k_{ls}$$

end

> Compute a Newton step:

$$\boldsymbol{\xi}_k = \boldsymbol{\xi}_k + \alpha\Delta\boldsymbol{\xi},$$
$$\boldsymbol{\lambda}_k = \boldsymbol{\lambda}_k + \alpha\Delta\boldsymbol{\lambda},$$
$$\boldsymbol{\mu}_k = \boldsymbol{\mu}_k + \alpha\Delta\boldsymbol{\mu},$$
$$\boldsymbol{s}_k = \boldsymbol{s}_k + \alpha\Delta\boldsymbol{s};$$

if $||\boldsymbol{r}_T||_2 \leq$ *threshold* **then**

break; (an approximate solution is found)

end

end

Output: $\boldsymbol{\xi}_k$

Instruments, where the control scheme is deployed on a dSPACE Microautobox II 1513/1514.

The tests are meant to show the accuracy of the current tracking at different operating points, the robustness against load variation, and the fast dynamic performance in transients while fulfilling the system constraints.

In Fig. 10, constant references of $i_q = 10$ A and $i_d = -2$ A were given, while the shaft speed stepped between 500 and 1500 r/min. It can be observed that, the speed variation is decoupled from the current tracking. It is noted that the current ripple is higher at 1500 r/min than at 500 r/min, that is because the parameter maps shown in Fig. 5 were obtained at 500 r/min. For machines that operate at a way higher speed range, the motor parameter maps have to be obtained at different speeds with the same procedure, and a 3-D LUT is to be used, i.e., letting the parameters be functions of i_d, i_q, and ω_{me}.

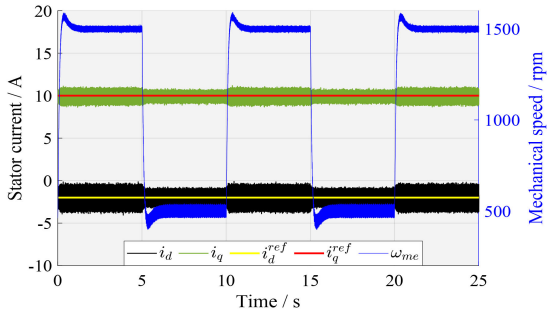

Fig. 10. Robustness test against speed variation.

The steady-state tracking results are presented in Fig. 11. Step changes for i_d^{ref} from -10 to -5 A to 0 A at a constant i_q^{ref} of 5 A were given. The tracking results of this scenario are depicted in Fig. 11(a) for $\omega_{\text{me}} = 250$ r/min, in Fig. 11(b) for $\omega_{\text{me}} = 500$ r/min, and in Fig. 11(c) for $\omega_{\text{me}} = 1000$r/min. In Fig. 11(d)–(f), step changes of i_q^{ref} from 15 A to 10 A to 5 A at constant i_d^{ref} of 0 A are shown at the same three different motor speeds of 250, 500, and 1000 r/min, respectively. The proposed CCS-MPC scheme proved to provide accurate tracking of both axes' currents at different speeds. However, at double the speed at which the model parameters were obtained, a slight offset is observed in Fig. 11(c). Thus, obtaining the model parameters at different speeds and interpolating in between them or having a simple steady-state integral action is a necessity for an offset-free performance over the whole speed range, even when a detailed nonlinear model is incorporated.

An essential benefit of using the nonlinear model is to gain the fastest possible performance in transients without significant over- or undershooting. This is illustrated from the transient test scenarios shown in Fig. 12. A step-up of i_q^{ref} from 1 to 17 A is commanded, and the results are shown at 500 and 1500 r/min in Fig. 12(a) and (c), respectively. Noting that the currents are measured in the *middle* of each sampling period, as explained in Section II-C, and with respect to the maximum available control input, as shown in Fig. 12(b) and (d) (i.e., the voltage amplitudes for the tests in Fig. 12(a) and (c), respectively), the fast dynamic response of the proposed controller with minimal over/undershoot and with fulfilling the input constraints is manifested. A step-down of i_d^{ref} from 0 to -12 A at 500 r/min is made in Fig. 12(e) with the corresponding voltage amplitude shown in Fig. 12(f), and the same at a speed of 1500 r/min is shown in Fig. 12(g) with the corresponding voltage in Fig. 12(h). Similar conclusions are drawn from the d-axis current transient.

B. Linear CCS-MPC for a SMPMSM

In this subsection, the proposed CCS-MPC scheme is implemented on a 14.5 kW SMPMSM using an LTI model. The motor parameters are $R_s = 0.15\ \Omega$, $L_d = L_q = 3.4$ mH, $\psi_p = 0.375$ Wb, $n_p = 3$ pole pairs, the nominal $\omega_{\text{me}} = 209$ rad $\cdot$ s^{-1}, and $u_{\text{dc}} = 560$ V. The test bench is depicted in Fig. 13. The sampling frequency is 8 kHz, and a prediction horizon $N = 2$ is used. The measured execution time T_{ex} is

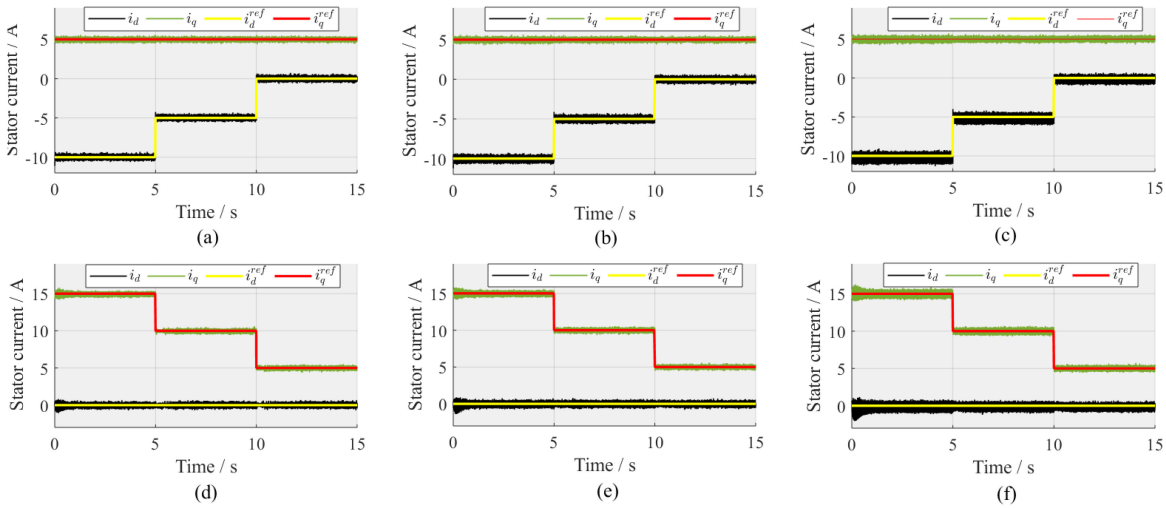

Fig. 11. Steady-state current tracking results using a CCS-MPC scheme based on the nonlinear model: i_d steps from -10 to -5 to 0 A at $i_q = 5$A at (a) 250 r/min, (b) 500 r/min, and (c) 1000 r/min, and i_q steps from 15 to 10 to 5 A at $i_d = 0$A at (d) 250 r/min, (e) 500 r/min, and (f) 1000 r/min.

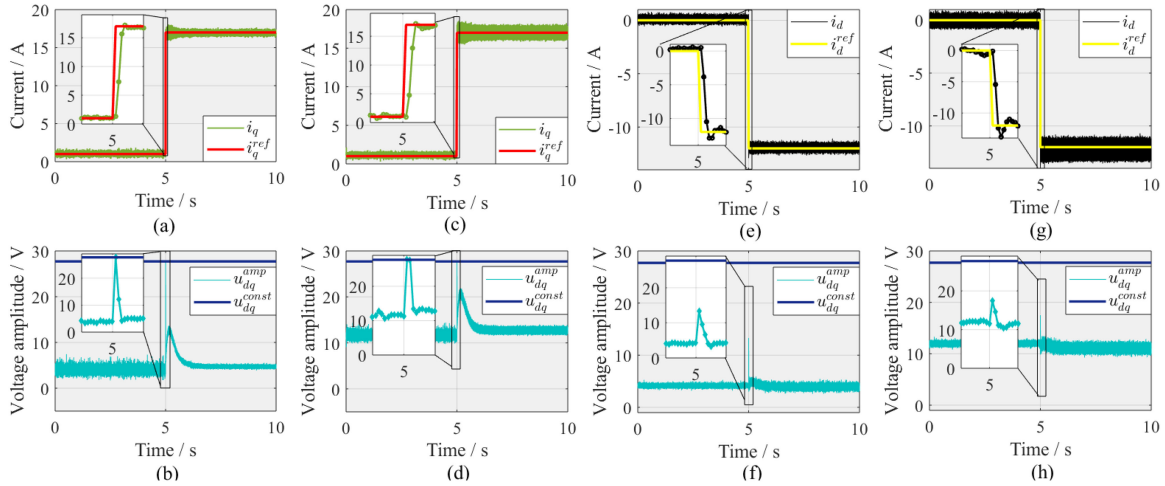

Fig. 12. Dynamic response using the proposed CCS-MPC scheme for a step-up change of i_q^{ref} from 1 to 17 A at 500 r/min is shown in (a) with the stator voltage amplitude and its constraint shown for that test in (b); the same test was repeated at 1500r/min, and the results are shown in (c) and (d); a step-down change of i_d^{ref} from 0 to -12 A at 500 r/min is shown in (e) with its stator voltage in (f); in (g) and (h), the same results are shown for the same step change at 1500 r/min.

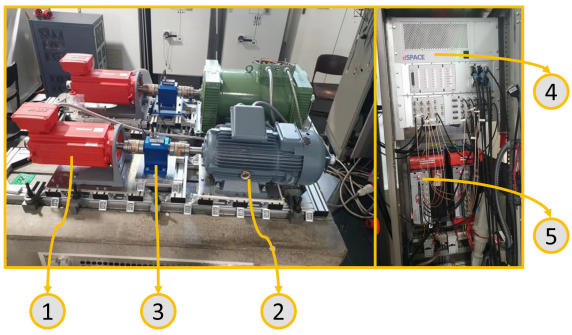

Fig. 13. SMPMSM test bench: 1) main motor (SMPMSM); 2) load motor (doubly fed induction motor); 3) torque sensor; 4) dSPACE DS1007; and 5) two-level VSI from SEW drives.

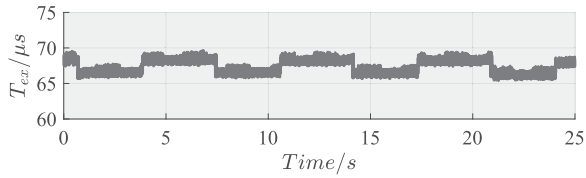

Fig. 14. Measured execution time of the proposed CCS-MPC scheme measured on the dSPACE DS1007 platform.

shown in Fig. 14. The experimental results were obtained once while using solely an LTI model of the plant and again while using a discrete-time integral action as an additive control input to compensate for the model mismatch. In Fig. 15(a), step changes of the reference torque producing current i_q^{ref} from 12 to 24 A at $i_d^{\text{ref}} = 0$ A and $\omega_{\text{me}} = 120$ rad $\cdot$ s^{-1} were given, while the motor is controlled by the CCS-MPC scheme without an integral action. Slight persistent offsets are observed. In Fig. 15(b), an

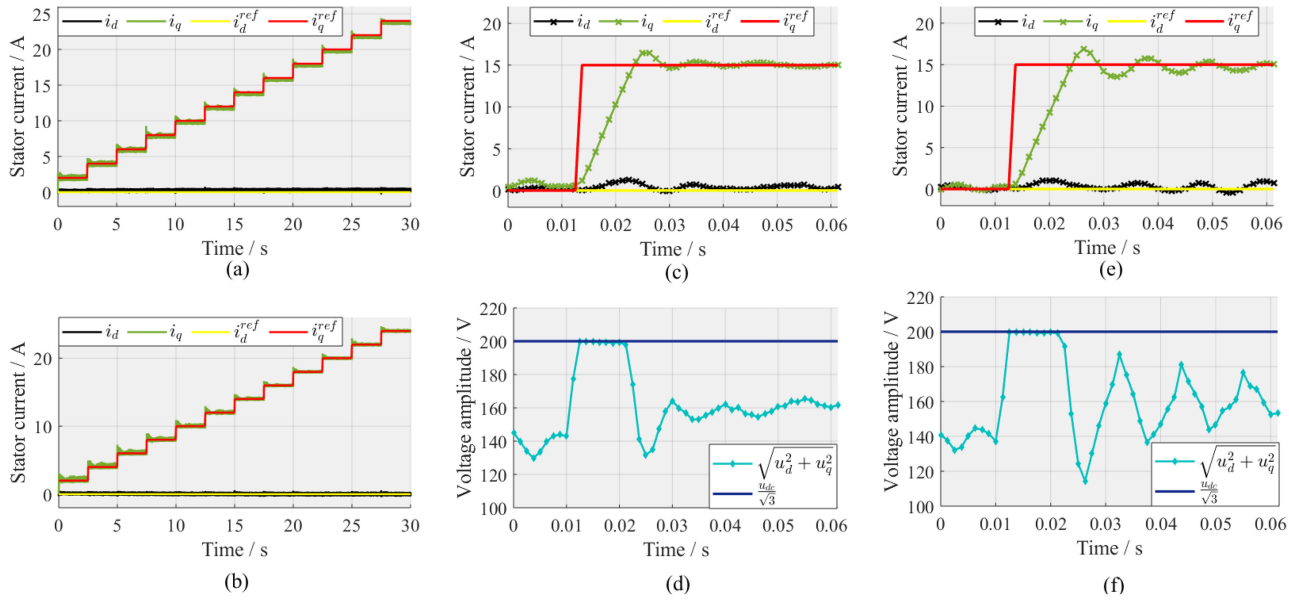

Fig. 15. Experimental results of the proposed CCS-MPC scheme on an SMPMSM. (a) Current tracking results using the LTI model without an integral action. (b) Current tracking results using the LTI model with an additive integral action term. (c) Step dynamic of i_q^{ref} from 0 to 15 A at $\omega_{\text{me}} = 120$ rad $\cdot$ s^{-1} with the LTI model and without integral action, and the corresponding voltage constraint fulfillment is depicted in (d), and in (e) and (f), the same step change was made with an integral action.

additive discrete-time integrating control input is added to the MPC control input for the same test scenario, and hence, an offset-free performance is obtained. To investigate the transient response of the linear MPC scheme with and without an integral action, and to check the input constraint fulfillment, the voltage amplitude is limited to 200 V and a step change of i_q^{ref} from 0 to 15 A is made at $\omega_{\text{me}} = 120$ rad $\cdot$ s^{-1}. The current tracking results of this test are shown for the linear MPC without an integrator in Fig. 15(c) with the voltage amplitude in Fig. 15(d), and for the linear MPC with an integral action in Fig. 15(e) and (f). The input constraints are completely fulfilled. The expense of using a simple LTI model appears again, as can be seen from the overshoot in the current tracking and the slight offset in i_d in Fig. 15(c). The offset-free performance obtained with the integral action besides the MPC comes at the expense of more fluctuations around the reference, as can be seen in Fig. 15(e), and the overshoot still persist to occur.

V. Conclusion

In this article, a CCS-MPC scheme for PMSMs based on the nonlinear first-principles model of the machine was proposed. The performance gain of using the nonlinear model was quantified over the widely used simple LTI models in MPC schemes for the control of electrical machines. The results obtained in this article motivated the use of the nonlinear modeling procedure presented in this article in order to obtain minimal steady-state ripples, tracking offsets, over/undershoot, and fast dynamic response with MPC controllers. The proposed control scheme based on the IP numerical solver was experimentally tested on an IPMSM and an SMPMSM. The experimental results showed that the proposed scheme is capable of being implemented in real time in the submillisecond range typically available for the current control loop of electrical machines and showed an optimal transient as well as steady-state performance, while fulfilling the system constraints.

Acknowledgment

Part of the experimental results was carried out at the Laboratory for Mechatronic and Renewable Energy Systems, Munich University of Applied Sciences, Munich, Germany.

References

[1] J. Gieras, *Permanent Magnet Motor Technology: Design and Applications*. New York, NY, USA: Taylor & Francis/CRC Press, 2010.

[2] F. Morel, X. Lin-Shi, J.-M. Retif, B. Allard, and C. Buttay, "A comparative study of predictive current control schemes for a permanent-magnet synchronous machine drive," *IEEE Trans. Ind. Electron.*, vol. 56, no. 7, pp. 2715–2728, Jul. 2009.

[3] E. F. Camacho, *Model Predictive Control*. Berlin, Germany: Springer, 2007.

[4] J. Holtz and S. Stadtfeld, "Field-oriented control by forced motor currents in a voltage fed inverter drive," *IFAC Proc. Vol.*, vol. 16, no. 16, pp. 103–110, 1983.

[5] R. Kennel, "Predictive control for power converters: Derivation and realization on microcomputer-based line-commutated converters," Ph.D. dissertation, Dept. Elect. Eng., Tech. Univ. Kaiserslautern, Kaiserslautern, Germany, 1984.

[6] D. Schröder and R. Kennel, "Model-control PROMC—A new control strategy with microcomputer for drive applications," *IEEE Trans. Ind. Appl.*, vol. IA-21, pp. 1162–1167, Sep. 1985.

[7] A. Linder and R. Kennel, "Model predictive control for electrical drives," in *Proc. IEEE 36th Power Electron. Spec. Conf.*, 2005, pp. 1793–1799.

[8] S. Kouro, P. Cortes, R. Vargas, U. Ammann, and J. Rodriguez, "Model predictive control—A simple and powerful method to control power converters," *IEEE Trans. Ind. Electron.*, vol. 56, no. 6, pp. 1826–1838, Jun. 2009.

[9] D. Quevedo, R. Aguilera, and T. Geyer, "Predictive control in power electronics and drives: Basic concepts, theory, and methods," in *Advanced and Intelligent Control in Power Electronics and Drives. Studies in Computational Intelligence*, vol. 531. Cham, Switzerland: Springer, 2014, pp. 181–226.

[10] T. Geyer, *Model Predictive Control of High Power Converters and Industrial Drives*. Hoboken, NJ, USA: Wiley, 2016.

[11] A. Andersson and T. Thiringer, "Assessment of an improved finite control set model predictive current controller for automotive propulsion applications," *IEEE Trans. Ind. Electron.*, vol. 67, no. 1, pp. 91–100, Jan. 2020.

[12] S. Wendel, A. Dietz, and R. Kennel, "FPGA based finite-set model predictive current control for small PMSM drives with efficient resource streaming," in *Proc. IEEE Int. Symp. Predictive Control Elect. Drives Power Electron.*, 2017, pp. 66–71.

[13] A. A. Ahmed, B. K. Koh, and Y. I. Lee, "Continuous control set-model predictive control for torque control of induction motors in a wide speed range," *Elect. Power Compon. Syst.*, vol. 46, nos. 19/20, pp. 2142–2158, 2018.

[14] A. K. Rathore, J. Holtz, and T. Boller, "Synchronous optimal pulsewidth modulation for low-switching-frequency control of medium-voltage multilevel inverters," *IEEE Trans. Ind. Electron.*, vol. 57, no. 7, pp. 2374–2381, Jul. 2010.

[15] T. Geyer, N. Oikonomou, G. Papafotiou, and F. D. Kieferndorf, "Model predictive pulse pattern control," *IEEE Trans. Ind. Appl.*, vol. 48, no. 2, pp. 663–676, Mar./Apr. 2012.

[16] P. Karamanakos, P. Stolze, R. M. Kennel, S. Manias, and H. du Toit Mouton, "Variable switching point predictive torque control of induction machines," *IEEE Trans. Emerg. Sel. Topics Power Electron.*, vol. 2, no. 2, pp. 285–295, Jun. 2014.

[17] P. Stolze, "Advanced finite-set model predictive control for power electronics and electrical drives," Ph.D. dissertation, Dept. Elect. Comput. Eng., Tech. Univ. Munich, Germany, Jan. 2014.

[18] L. Wang, T. Zhao, and J. He, "Investigation of variable switching frequency in finite control set model predictive control on grid-connected inverters," *IEEE Open J. Ind. Appl.*, vol. 2, pp. 178–193, 2021.

[19] P. Karamanakos, E. Liegmann, T. Geyer, and R. Kennel, "Model predictive control of power electronic systems: Methods, results, and challenges," *IEEE Open J. Ind. Appl.*, vol. 1, pp. 95–114, 2020.

[20] I. Hammoud, S. Hentzelt, T. Oehlschlaegel, and R. Kennel, "Modelling for nonlinear predictive control of synchronous machines: First principles vs. data-driven approaches," in *Proc. 6th IEEE Int. Conf. Predictive Control Elect. Drives Power Electron.*, 2021, pp. 715–724.

[21] T. Englert and K. Graichen, "Nonlinear model predictive torque control of PMSMs for high performance applications," *Control Eng. Pract.*, vol. 81, pp. 43–54, 2018.

[22] T. Englert and K. Graichen, "Nonlinear model predictive torque control and setpoint computation of induction machines for high performance applications," *Control Eng. Pract.*, vol. 99, 2020, Art. no. 104415.

[23] G. Cimini, D. Bernardini, A. Bemporad, and S. Levijoki, "Online model predictive torque control for permanent magnet synchronous motors," in *Proc. IEEE Int. Conf. Ind. Technol.*, 2015, pp. 2308–2313.

[24] G. Cimini, D. Bernardini, S. Levijoki, and A. Bemporad, "Embedded model predictive control with certified real-time optimization for synchronous motors," *IEEE Trans. Control Syst. Technol.*, vol. 29, no. 2, pp. 893–900, Mar. 2021.

[25] A. Zanelli, J. Kullick, H. M. Eldeeb, G. Frison, C. M. Hackl, and M. Diehl, "Continuous control set nonlinear model predictive control of reluctance synchronous machines," *IEEE Trans. Control Syst. Technol.*, vol. 30, no. 1, pp. 130–141, Jan. 2021.

[26] C. J. O'Rourke, M. M. Qasim, M. R. Overlin, and J. L. Kirtley, "A geometric interpretation of reference frames and transformations: Dq0, clarke, and park," *IEEE Trans. Energy Convers.*, vol. 34, no. 4, pp. 2070–2083, Dec. 2019.

[27] C. Hackl, *Non-identifier Based Adaptive Control in Mechatronics*, vol. 466. Berlin, Germany: Springer, 2017.

[28] S. L. Kellner, "Parameteridentifikation bei permanenterregten synchronmaschinen," Ph.D. dissertation, Dept. Elect., Elect. Inf. Technol., Friedrich-Alexander Univ. Erlangen-Nürnberg, Erlangen, Germany, 2012.

[29] S. L. Kellner and B. Piepenbreier, "General PMSM d,q-model using optimized interpolated absolute and differential inductance surfaces," in *Proc. IEEE Int. Elect. Mach. Drives Conf.*, 2011, pp. 212–217.

[30] S. Ebersberger and B. Piepenbreier, "Identification of differential inductances of permanent magnet synchronous machines using test current signal injection," in *Proc. Int. Symp. Power Electron. Power Electron. Elect. Drives, Autom. Motion*, 2012, pp. 1342–1347.

[31] I. Hammoud, S. Hentzelt, T. Oehlschlaegel, and R. Kennel, "Long-horizon direct model predictive control based on neural networks for electrical drives," in *Proc. 46th Annu. Conf. IEEE Ind. Electron. Soc.*, 2020, pp. 3057–3064.

[32] L. L. Schumaker, *Spline Functions: Computational Methods*. Philadelphia, PA, USA: SIAM, 2015.

[33] I. Hammoud, S. Hentzelt, T. Oehlschlaegel, and R. Kennel, "Learning-based model predictive current control for synchronous machines: An LSTM approach," in *Proc. Eur. Control Conf.*, 2022, pp. 1–8.

[34] B.-H. Bae and S.-K. Sul, "A compensation method for time delay of full-digital synchronous frame current regulator of PWM AC drives," *IEEE Trans. Ind. Appl.*, vol. 39, no. 3, pp. 802–810, May/Jun. 2003.

[35] M. Abdelrahem, C. M. Hackl, R. Kennel, and J. Rodríguez, "Efficient direct-model predictive control with discrete-time integral action for PMSGs," *IEEE Trans. Energy Convers.*, vol. 34, no. 2, pp. 1063–1072, Jun. 2019.

[36] I. Hammoud, K. Xu, S. Hentzelt, T. Oehlschlaegel, and R. Kennel, "On offset-free continuous model predictive current control of permanent magnet synchronous motors," *IFAC-PapersOnLine*, vol. 53, no. 2, pp. 6662–6669, 2020.

[37] H. Xu, X. Gui, T. Luan, X. Lang, and D. Xu, "A robust predictive current controller with incremental model and inductance observer for PMSM drive," in *Proc. IEEE Transp. Electrific. Conf. Expo*, 2017, pp. 1–6.

[38] X. Zhang, L. Zhang, and Y. Zhang, "Model predictive current control for PMSM drives with parameter robustness improvement," *IEEE Trans. Power Electron.*, vol. 34, no. 2, pp. 1645–1657, Feb. 2019.

[39] J. Oravec, M. Bakošová, L. Hanulová, and M. Horváthová, "Design of robust MPC with integral action for a laboratory continuous stirred-tank reactor," in *Proc. 21st Int. Conf. Process Control*, 2017, pp. 459–464.

[40] T. Badgwell and K. Muske, "Disturbance model design for linear model predictive control," in *Proc. Amer. Control Conf.*, 2002, vol. 2, pp. 1621–1626.

[41] K. R. Muske and T. A. Badgwell, "Disturbance modeling for offset-free linear model predictive control," *J. Process Control*, vol. 12, no. 5, pp. 617–632, 2002.

[42] U. Maeder, F. Borrelli, and M. Morari, "Linear offset-free model predictive control," *Automatica*, vol. 45, no. 10, pp. 2214–2222, 2009.

[43] G. Pannocchia and E. C. Kerrigan, "Offset-free receding horizon control of constrained linear systems," *AIChE J.*, vol. 51, pp. 3134–3146, 2005.

[44] M. Norambuena, P. Lezana, and J. Rodriguez, "A method to eliminate steady-state error of model predictive control in power electronics," *IEEE Trans. Emerg. Sel. Topics Power Electron.*, vol. 7, no. 4, pp. 2525–2530, Dec. 2019.

[45] X. Liu, L. Zhou, J. Wang, X. Gao, Z. Li, and Z. Zhang, "Robust predictive current control of permanent-magnet synchronous motors with newly designed cost function," *IEEE Trans. Power Electron.*, vol. 35, no. 10, pp. 10 778–10 788, Oct. 2020.

[46] X. Li, W. Tian, X. Gao, Q. Yang, and R. Kennel, "A generalized observer-based robust predictive current control strategy for PMSM drive system," *IEEE Trans. Ind. Electron.*, vol. 69, no. 2, pp. 1322–1332, Feb. 2022.

[47] O. Wallscheid and E. F. B. Ngoumtsa, "Investigation of disturbance observers for model predictive current control in electric drives," *IEEE Trans. Power Electron.*, vol. 35, no. 12, pp. 13 563–13 572, Dec. 2020.

[48] J. Maciejowski, *Predictive Control With Constraints*. Englewood Cliffs, NJ, USA: Prentice-Hall, 2002.

[49] Z. Q. Zhu, D. Liang, and K. Liu, "Online parameter estimation for permanent magnet synchronous machines: An overview," *IEEE Access*, vol. 9, pp. 590 59–59 084, 2021.

[50] X. Li and R. Kennel, "Comparison of state-of-the-art estimators for electrical parameter identification of PMSM," in *Proc. IEEE Int. Symp. Predictive Control Elect. Drives Power Electron.*, 2019, pp. 1–6.

[51] A. Glac, V. Šmídl, Z. Peroutka, and C. M. Hackl, "Comparison of IPMSM parameter estimation methods for motor efficiency," in *Proc. 46th Annu. Conf. IEEE Ind. Electron. Soc.*, 2020, pp. 895–900.

[52] M. Schmidt, "An interior-point method for nonlinear optimization problems with locatable and separable nonsmoothness," *EURO J. Comput. Optim.*, vol. 3, no. 4, pp. 309–348, Nov. 2015.

[53] Y. Wang and S. Boyd, "Fast model predictive control using online optimization," *IEEE Trans. Control Syst. Technol.*, vol. 18, no. 2, pp. 267–278, Mar. 2010.

[54] A. Malyshev, R. Quirynen, and A. Knyazev, "Preconditioned Krylov iterations and condensing in interior point MPC method," *IFAC-PapersOnLine*, vol. 51, no. 20, pp. 388–393, 2018.

Issa Hammoud (Student Member, IEEE) received the B.Sc. degree in energy engineering from German Jordanian University, Amman, Jordan, in 2016, and the M.Sc. degree in power engineering (with distinction) in 2018 from the Technical University of Munich, Munich, Germany, where he is currently working toward the Ph.D. degree in electrical engineering with the Institute for Electrical Drive Systems and Power Electronics.

He is also with the Powertrain Mechatronics Control Engineering Excellence Cluster, IAV GmbH, Gifhorn, Germany. His current research interests include nonlinear predictive control of electric and renewable energy systems and the use of artificial intelligence methods in power electronic applications.

Dr. Hammoud received the best paper awards at the Fifth and Sixth International Symposium on Predictive Control of Electrical Drives and Power Electronics in 2019 and 2021, respectively.

Sebastian Hentzelt received the Diploma degree in systems engineering and engineering cybernetics from Otto-von-Guericke University in Magdeburg, Magdeburg, Germany, in 2010, and the Ph.D. degree in control engineering from Ulm University, Ulm, Germany, in 2021.

From 2011 to 2016, he was part of the academic staff with the Institute of Measurement, Control and Microtechnology, Ulm University. Since 2016, he has been with the Powertrain Mechatronics Control Engineering Excellence Cluster, IAV GmbH, Gifhorn, Germany. His research interests include distributed nonlinear model predictive control, general nonlinear predictive control methods, and data-driven modeling methods.

Ke Xu received the M.Sc. degree in mechanical engineering (with distinction) from Paderborn University, Paderborn, Germany, in 2014.

From October 2014 to July 2018, he was part of the academic stuff with the Control Engineering Group, Heinz Nixdorf Institute, Paderborn University. Since July 2018, he has been with the Powertrain Mechatronics Control Engineering Excellence Cluster, IAV GmbH, Gifhorn, Germany. His main research interests include motion planning, nonlinear and optimal control, model predictive control, and numerical optimization algorithms.

Thimo Oehlschlägel received the Diploma degree in process engineering from the Technical University of Clausthal, Clausthal-Zellerfeld, Germany, in 2003, and the Ph.D. degree in control theory from the Institute of Automatic Control and Mechatronics, Technische Universität Darmstadt, Darmstadt, Germany, in 2015.

From 2009 to 2015, he was with German Aerospace Center, Bremen, Germany. Since 2018, he has been leading the Powertrain Mechatronics Control Engineering Excellence Cluster, IAV GmbH, Gifhorn, Germany. His research interests include robust control, model predictive control, and guidance, navigation, and control for autonomous systems.

Mohamed Abdelrahem (Senior Member, IEEE) was born in Assiut, Egypt, in 1985. He received the B.Sc. (Hons.) and M.Sc. degrees from Assiut University, Assiut, Egypt, in 2007 and 2011, respectively, and the Ph.D. degree (with distinction) from the Technical University of Munich (TUM), Munich, Germany, in 2020, all in electrical engineering.

Since 2019, he has been the Head of the Research Group "Renewable Energy Systems," Institute for Electrical Drive Systems and Power Electronics, TUM. His research interests include power electronics, predictive and encoderless control of variable-speed wind generators, photovoltaic energy systems, and energy storage systems.

Dr. Abdelrahem is the recipient of several best paper awards from international IEEE conferences.

Christoph Hackl (Senior Member, IEEE) was born in Mannheim, Germany, in 1977. He received the B.Sc., Dipl.-Ing., and Dr.Ing. (Ph.D.) degrees in electrical engineering from the Technical University of Munich (TUM), Munich, Germany, in 2003, 2004, and 2012, respectively.

He studied electrical engineering (with focus on mechatronics and systems and control) with TUM and the University of Wisconsin–Madison, Madison, WI, USA. Since 2004, he has been teaching electrical drives, power electronics, and mechatronic and renewable energy systems. Since 2014, he has been the Head of the Research Group "Control of Renewable Energy Systems," TUM. In 2018, he became a Professor of Electrical Machines and Drives and the Head of the Laboratory for Mechatronic and Renewable Energy Systems, Munich University of Applied Sciences (MUAS), Munich. In 2019, he completed his habilitation on "Mechatronic and Renewable Energy Systems" and co-founded the research Institute for Sustainable Energy Systems, MUAS. His research interests include nonlinear, adaptive, and optimal control and design of electrical drives and mechatronic and renewable energy systems.

Ralph Kennel (Senior Member, IEEE) was born in Kaiserslautern, Germany, in 1955. He received the Diploma and Ph.D. degrees in electrical machines and drives from the University of Kaiserslautern, Kaiserslautern, in 1979 and 1984, respectively.

From 1983 to 1999, he was with Robert Bosch GmbH, Gerlingen, Germany. From 1994 to 1999, he was a visiting Professor with the University of Newcastle upon Tyne, Newcastle upon Tyne, U.K. From 1999 to 2008, he was a Professor of Electrical Machines and Drives with the University of Wuppertal, Wuppertal, Germany. Since 2008, he has been the Head of the Chair of Electrical Drive Systems and Power Electronics, Technical University of Munich, Munich, Germany. His main research interests include model predictive control in the field of power electronics and electrical drives, sensorless control of ac drives, and hardware-in-the-loop systems.

Prof. Kennel received the Harry Owen Distinguished Service Award from the IEEE Power Electronics Society (PELS) in 2013, the EPE Association Outstanding Service Award in 2015, and the EPE Outstanding Achievement Award in 2019. He received the honorary doctorate degree from Ştefan cel Mare University of Suceava, Suceava, Romania, in 2018. He is a Fellow of the Institution of Engineering and Technology and a Chartered Engineer in the U.K. Within the IEEE, he is Treasurer of the Germany Section and the ECCE Global Partnership Chair of the IEEE PELS.